Pharmaceutical Biology

ISSN: 1388-0209 (Print) 1744-5116 (Online) Journal homepage: http://www.tandfonline.com/loi/iphb20

Lauric acid and myristic acid from Allium sativum inhibit the growth of Mycobacterium tuberculosis H37Ra: in silico analysis reveals possible binding to protein kinase B

Rajiniraja Muniyan & Jayaraman Gurunathan

To cite this article: Rajiniraja Muniyan & Jayaraman Gurunathan (2016): Lauric acid and myristic acid from Allium sativum inhibit the growth of Mycobacterium tuberculosis H37Ra: in silico analysis reveals possible binding to protein kinase B, Pharmaceutical Biology, DOI: 10.1080/13880209.2016.1184691

To link to this article: http://dx.doi.org/10.1080/13880209.2016.1184691

Published online: 16 Jun 2016.

PHARMACEUTICAL BIOLOGY, 2016
http://dx.doi.org/10.1080/13880209.2016.1184691

Taylor & Francis
Taylor & Francis Group

RESEARCH ARTICLE

Lauric acid and myristic acid from *Allium sativum* inhibit the growth of *Mycobacterium tuberculosis* H37Ra: *in silico* analysis reveals possible binding to protein kinase B

Rajiniraja Muniyan and Jayaraman Gurunathan

School of Bio Sciences and Technology, VIT University, Vellore, Tamil Nadu, India

ABSTRACT

Context: The bulb of *Allium sativum* Linn (Alliaceae) has numerous medicinal values. Though the petroleum ether extract of the bulb has shown to exhibit antimycobacterial activity, the phytochemical(s) responsible for this inhibitory activity is not known.

Objective: To characterize the bioactive compounds in the petroleum ether extract of *Allium sativum* (garlic) that inhibit the growth of *Mycobacterium tuberculosis* H37Ra.

Materials and methods: Bioactivity-guided fractionation was employed to isolate the bioactive compounds. Antimycobacterial activity was evaluated by well-diffusion method and microplate alamar blue assay (MABA). Infrared spectroscopy, mass spectrometry and nuclear magnetic resonance spectroscopy were used to characterize the bioactive compounds. Autodock was used to obtain information on molecular recognition, and molecular dynamics simulation was performed using GROMACS.

Results: The bioactive compounds that inhibited the growth of *M. tuberculosis* H37Ra were found to be lauric acid (LA) and myristic acid (MA). The minimal inhibitory concentration of LA and MA was found to be 22.2 and 66.7 μg/mL, respectively. *In silico* analysis revealed that these fatty acids could bind at the cleft between the N-terminal and C-terminal lobes of the cytosolic domain of serine/threonine protein kinase B (PknB).

Discussion and conclusion: The inhibition activity was dependent on the alkyl chain length of the fatty acid, and the amino acid residues involved in binding to fatty acid was found to be conserved across the Pkn family of proteins. The study indicates the possibility of using fatty acid derivatives, involving Pkn family of proteins, to inhibit the signal transduction processes in *M. tuberculosis*.

ARTICLE HISTORY
Received 30 June 2015
Revised 21 January 2016
Accepted 27 April 2016
Published online 14 June 2016

KEYWORDS
Bioactivity-guided fractionation; microplate Alamar blue assay; petroleum ether extract; molecular dynamic simulations; spectroscopic analysis

Introduction

Tuberculosis (TB) caused by *Mycobacterium tuberculosis* is one of the most prolific infectious disease with high mortality worldwide (Dye et al. 1999). In 2013, 8.6 million people were estimated to develop TB, of whom 1.3 million died (including 360,000 deaths among HIV-positive) [Global Tuberculosis Report, World Health Organization (WHO), 2013]. Annual reports indicate that the number of multidrug-resistant (MDR) cases is on the rise (Global Tuberculosis Report, WHO, 2014). Therefore, it is necessary to look for alternate strategies to combat this infectious bacterium.

Medicinal plants are being used worldwide by traditional healers to treat various ailments, including infectious diseases. Literature indicates that the primary sources of 65–75% medicines used today are plants (Newton et al. 2000). Extracts of various common herbal plants have been shown to exhibit antimycobacterial activity. Gebreyohannes and Gebreyohannes (2013) recently reviewed the medicinal values of *Allium sativum* Linn (Alliaceae) and documented that the extracts of this common plant have potential pharmaceutical application for the treatment of heart diseases, hypertension, cancer, diabetics, inflammation, atherosclerosis, hyperlipidaemia, viral and microbial infections.

Allicin from *A. sativum* inhibits the growth of *M. tuberculosis in vitro* (Schauenberg & Paris 1990; Gupta et al. 2011), but loses its beneficial properties within an hour as it rapidly gets oxidized to diallyl sulfides, diallyl disulfides, diallyl trisulfides, vinyl dithiins and ajoenes. Geraniol, from the same plant but at higher concentration, also inhibits the growth of *M. tuberculosis* (Dini et al. 2011). The *in vivo* antimycobacterial activity of garlic oil was studied in tubercle bacilli-exposed guinea pigs and it was comparable with the acivity of first-line drugs such as streptomycin and rifampicin (Jain 1998). The pharmacological activity of garlic and the phytochemicals therein are being studied for the past three decades, of which the organosulphur compounds, especially allicin is one among the most-studied compounds (Mikaili et al. 2013). Apart from the antimicrobial activity, the selected sulphur compounds from garlic have found to induce apoptosis by suppressing NF-kB signaling through destabilization of TRAF6 in primary effusion lymphoma (Shigemi et al. 2016); attenuates oxidation stress, inflammation and endothelial dysfunction in hypercholesterolemic rabbits (El-Sheakh et al. 2016) and protects against ischemic stroke in a rat model (Zhang et al. 2015).

We have shown, recently, that the petroleum ether extract of the bulb of *A. sativum* inhibits the growth of *M. tuberculosis* H37Ra. Since the initial analysis revealed that the phytochemical responsible for the inhibition activity could be different from allicin and geraniol (Rajiniraja & Jayaraman 2014), the present study aimed to isolate and characterize the active compounds from the bulbs of *A. sativum* using various analytical techniques and to

CONTACT Jayaraman Gurunathan gjayaraman@vit.ac.in School of Bio Sciences and Technology, VIT University, Vellore 632014, Tamil Nadu, India
Supplemental data for this article can be accessed here.

arrive at a possible mechanism of action through molecular modelling and simulations.

Materials and methods

Chemicals

Petroleum ether, chloroform-AR, rifampicin were purchased from SDF Chem. Ltd (Gujarat, India); Silica gel 230–400 mesh from HiMedia (Mumbai, India); Alamar Blue, 96-well micro titre plate, Loewenstein-Jensen medium base from Fluka-63237 (Bangalore, India); Middlebrook 7H9 broth base from Accumix^{TM} (Bangalore, India); glycerol, lauric acid (LA), myristic acid, palmitic acid and stearic acid were purchased from Sigma-Aldrich (Bangalore, India).

Preparation of petroleum ether extract

Allium sativum (garlic) bulbs were purchased from the local market (Vellore, Tamil Nadu, India) on September 2011. The bulbs were authenticated by Dr. K. Madhava Chetty and a specimen (Voucher no. 2011) was deposited at the herbarium of Sri Venkateswara University, Tirupati, India.

The bulb was peeled, washed with double-distilled water, chopped into small pieces, air dried in shade at room temperature (25 °C) for two weeks and then ground into fine paste. The paste was stored in sterile bag at 4 °C until use (Harborne 1973).

The non-polar components in the above paste were extracted (40 °C, 9 h) with petroleum ether (250 mL) using Soxhlet apparatus. The extract was then evaporated to dry using rotary evaporator (40 °C) and was stored in sterile bottle (covered with aluminum foil) as reported earlier (Chaudhar 1996; Rajiniraja & Jayaraman 2014).

Experimental design

Column chromatography

The petroleum ether extract (0.5 g) of *A. sativum* was subjected to column chromatography (1.5 x 54 cm; 15 g of silica gel 230–400 mesh) and the extracts were eluted using a step gradient of petroleum ether and chloroform (10:0, 9.5:0.5, 9:1, 8.5:1.5, 8:2, 7.5:2.5, 7:3, 6.5:3.5, 6:4, 0:10 each 1 L). Fractions were transferred into tightly capped sterile glass bottles and stored at 4 °C until further use (Patra et al. 2012).

High-performance liquid chromatography

Column chromatographic fractions that exhibited antimycobacterial activity were subjected to HPLC (LC-8A prominence and Rheodyne type injector, Shimadzu Corporation, Japan). Phenomenex Luna (250 mm x 10 mm) column was used and elution was done in a reverse-phase mode at ambient temperature. The elution was performed in isocratic mode with acetonitrile:-water (60:40), flow rate of 8.6 mL/min and detection wavelength of 220 nm. The fractions were collected, evaporated to dryness and stored (at 4 °C) in a sterile glass bottle.

Culture medium and organism growth

Mycobacterium tuberculosis H37Ra (MTCC 300) was purchased from IMTECH, Chandigarh (India). The organism was sub-cultured by suspending 6.2g of the Loewenstein–Jensen medium base in 100 mL water containing 2 mL glycerol and autoclaved at 15 lbs for 15 min. Egg emulsion (50 mL) was mixed with the base to obtain uniform mixture. The medium was aliquoted (10 mL) in sterile screw capped bottles and was made to coagulate by heating it at 85–90 °C for 45 min (NCIM). After solidification, *M. tuberculosis* was streaked (one loop full) and incubated at room temperature for 4 weeks.

The pure culture was isolated from the slant (LJ medium) and inoculated into 5 mL Middlebrook 7H9 broth base (Middlebrook & Cohn 1958) supplemented with 10% (v/v) albumin dextrose catalase (Accumix^{TM}) and 0.2% (v/v) glycerol (Sigma-Aldrich). The inoculated media was maintained at 37 °C for 72 h on a shaker until an OD_{600} of 0.6–0.8 was reached (equivalent to 3.2×10^7 cfu/mL).

Mycobacterium tuberculosis *assay*

In order to obtain the qualitative information on the antimycobacterial activity of the extracts agar well diffusion assay was performed (Parish & Stroker 1998, Molina-Salinas et al. 2007, Kouznetsov & Sánchez 2010; Rajiniraja & Jayaraman 2014). In all these experiments rifampicin (5 µg/mL) served as a positive control.

Determination of minimum inhibitory concentration

MIC was determined by microplate Alamar blue assay (MABA) in a 96-well micro titre plate. To 180 µL of freshly cultured medium, 20 µL of the sample (2–20 µg) was added. Rifampicin (5 µg) was used as the positive control. The plate was incubated at 37 °C for 48 h and 10 µL of Alamar blue was served into the wells (total volume of 210 µL). The MIC was defined as the lowest concentration of the extract in which the change in colour from blue to pink was not observed (Collins & Franzblau 1997; Prescott et al. 1999).

EI-MS, IR and NMR spectroscopy analysis

Electron impact-mass spectrometry (EI-MS) was carried out using JEOL GCMATE II GC-MS (Tokyo, Japan) with EI mode of ionization. The Fourier transform-infrared (FT-IR) spectra were recorded using a Perkin–Elmer instrument in the range of 400–4000 cm^{-1} in thallium bromide. Nuclear magnetic resonance (NMR) spectra were acquired on Bruker Accent multi nuclei probe spectrophotometer at 400 MHz (^1H, ^{13}C). Chemical shifts (δ ppm) were referenced with respect to tetra methyl silane (TMS). The spectra (^1H, ^{13}C, DEPT, COSY and HSQC) were recorded in $CDCl_3$ (Lanos et al. 2012).

Docking of fatty acids to PknB and PstP

The three-dimensional structures of serine/threonine protein kinase B (PknB) (PDB ID: 1MRU) and phosphatase (PDB ID: 2CM1) were retrieved from the Protein Data Bank. Since the structure of PknB (1MRU) lacked the region spanning from Ile163 to Thr179, the conformation of the missing region was predicted using Phyre2 (Protein fold recognition server: http://www.sbg.bio.ic.ac.uk/phyre2/html/page.cgi?id=index). The full-length protein was used for docking studies.

Docking of PknB and protein serine/threonine phosphatase (PstP) with the ligand was performed by Autodock (4.0) using the

Lamarckian genetic algorithm (Hu & Shelver 2003). The active site was defined using AutoGrid. The grid size was set to $90 \times 90 \times 90$ points with a grid spacing of 0.375 Å, centered on the binding site of the protein molecules (Dario & Roberto 2009). The grid box included the entire protein molecule to ensure enough space for the ligand translational and rotational walk. Step sizes of 1 Å for translation and 50° for rotation were chosen and the maximum number of energy evaluations was set to 54,00,000. One hundred runs were performed for each ligand. For each of the 100 independent runs, the genetic algorithm was set to generate 27 000 operations on a single population of 200 individuals. Default values were used for crossover, mutation and elitism operator weights (0.80, 0.02, and 1.00, respectively). Docked conformations of 100 runs were clustered on the basis of their root mean square deviation (RMSD) tolerance of the ligand conformation. Consequently, the best docked conformation was selected and visualized using Pymol 0.99 (New York, NY).

Molecular dynamics simulation

Molecular dynamics (MD) simulation of the free and ligand-bound protein was carried out with the GROMACS (Groningen, Netherland) 4.5.3 package using GROMOS96 force field (Berendsen et al., 1995; Schuler et al., 2001). The conformation of the protein–ligand complex with lowest binding energy (most negative) was used for MD simulation. The topology parameters for the proteins were created by using the GROMACS program. The topology parameters of the ligand were built using the Dundee PRODRG server (Scotland, UK) (Schuttelkopf & Van Aalten, 2004). The entire scheme was subjected to MD production run at a temperature of 300 K and a pressure of 1 bar for 5000 ps.

Table 1. Chromatographic fractions of petroleum ether extract of *A. sativum* Linn (Alliaceae).

Pooled fractions	Yield (mg)	Yield (%)	R_f value	Antimycobacterial activity
P_1	4.3	0.8	0.99	–
P_2	24.5	4.9	0.99	–
P_3	32.2	6.4	0.99, 0.84	–
P_4	26.4	5.2	0.84	–
P_5	29.8	5.9	0.72	–
P_6	36.8	7.3	0.62	–
P_7	34.0	6.8	0.46,	–
P_8	46.5	9.3	0.46, 0.21	–
P_9	96.6	19.3	0.21, 0.1	+++
P_{10}	58.9	11.7	0.01	++
P_{11}	64.5	12.9	0.01	+

Of the eleven fractions, only P_9 exhibited significant antimycobacterial activity (mentioned in bold). Presence of activity is shown as '+' whereas absence of activity is indicated as '–'. The retention factor values mentioned is for the TLC plates developed with petroleum ether: chloroform (4:1).
+ = 15–20 ± 0.5 of zone size (mm), ++ = 21–25 ± 0.5 (mm), +++ = 26–30 ± 0.5 (mm).

Results

Bioactivity-guided fractionation

The petroleum ether extract of *A. sativum* was recently shown to exhibit antimicrobial property against selected microorganisms, including *M. tuberculosis* H37Ra (Rajiniraja & Jayaraman 2014). In continuation of our efforts to investigate the nature of the active component, we embarked on purifying the petroleum ether extract of *A. sativum* by chromatographic techniques. The fractions collected were pooled (P_1–P_{11}) based on the R_f value and the homogeneity observed on the TLC plates. The fraction P_9 exhibited a significant antimycobacterial activity (Supplementary Figure 1). The yield (19.3% DW of the petroleum ether extract) of this component was apparently the highest (Table 1).

The EI-MS obtained, for P_9, in the positive-ion mode displayed peaks at *m/z* 200, 228, 256 and 283 (Figure 1) with their relative intensity (%) as 15, 10, 4, and 2, respectively. The difference of 28 in the *m/z* value between the subsequent peaks is suggestive of the presence of long chain aliphatic compounds.

TLC and HPLC analysis indicated that the active fraction, P_9, contained more than one component (Supplementary Figures 2–4) and therefore subsequent fractionation was performed with semi-preparative reverse-phase HPLC (Supplementary Figure 5). The one-dimensional (1D) proton NMR of the subfractions that displayed antimycobacterial activity (F_3–F_5), were not identical but had similar peak patterns. This indicated that the phytochemicals present in these subfractions could be of similar chemical nature. In addition, the spectral range of the chemical shifts (0.75–2.50 ppm) indicated that these compounds could be aliphatic, which corroborate with the mass spectral data. Table 2

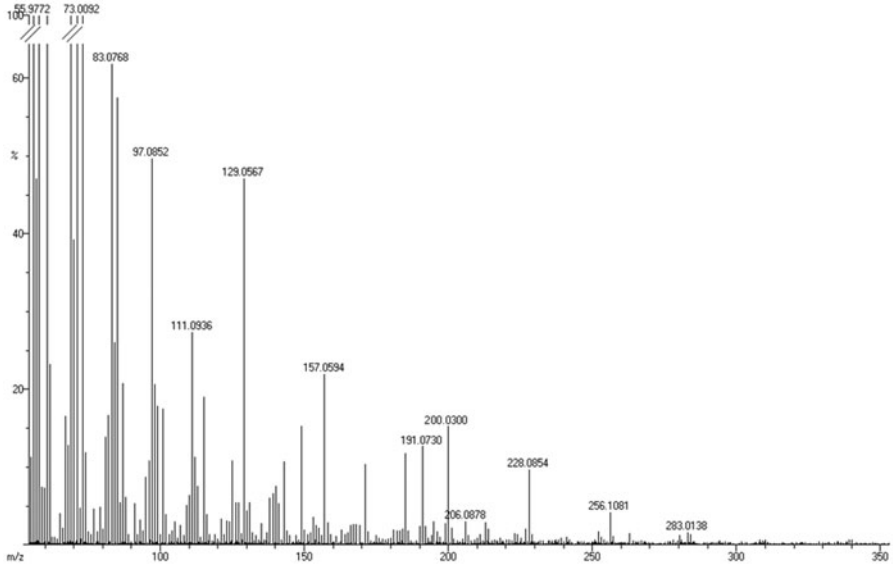

Figure 1. EI-MS for bioactive P_9 fraction was obtained in the positive ionization mode.

summarizes the steps involved in the purification of the active component. The overall yield and purification fold of the bioactive component (subfraction F_3) was found to be 31.0 mg (31.95% DW with respect to P_9) and 43, respectively.

Determination of the minimal inhibitory concentration (MIC) of the subfractions was performed, as per MABA (Supplementary Figure 6). The MIC of the subfractions F_3 and F_4 were found to be 22.2 and 66.7 µg/mL (Table 3), which are lower than the value reported for allicin and comparable with geraniol (Delaha & Garagusi 1985; Bueno-Sánchez et al. 2009).

IR, mass spectrometric and NMR spectroscopic analysis

The bioactive component in subfraction (F_3) was found to be colourless and odourless solid substance. The FT-IR spectrum (Figure (2a)) showed absorptions for aliphatic C–H stretches (at 2911 and 2845 cm^{-1}) and one carbonyl stretch at 1690 cm^{-1}. Such spectral characteristics indicated that the compound could be aliphatic carbonyl/carboxyl compound. EI-MS displayed peaks at *m/z* 200 with the relative intensity of 38% (Figure 2(b)). The molecular ion is clearly abundant, and there are ions representing fragmentations of methylene groups.

In order to get further insight into the nature of the active compound (in F_3 fraction), various one-dimensional (1D) and two-dimensional (2D) experiments were performed. The resonances in ^{1}H (0.75–2.5 ppm) and ^{13}C-NMR (20–40 ppm) (Supplementary Figures 7) confirmed the presence of a long chain aliphatic group in the active compound. Presence of carbonyl was inferred from the signal at 180 ppm in ^{13}C-NMR. The scalar connectivities obtained from the 2D experiments, COSY (Figure (2c)) and HSQC (Figure (2d)), confirmed that the active molecule in the F_3 fraction to be LA. The chemical shifts of ^{1}H and ^{13}C values are given in Supplementary Table 1. Similarly, the bioactive compound in the subfractions F_4 and F_5 were identified to be myristic acid (MA) and palmitic acid, respectively (Supplementary Figures 8).

Table 2. Purification process of the petroleum ether extract of *A. sativum* with information on yield, specific inhibition activity and purification fold.

Purification process	Yield (mg)	Specific inhibition activity by plate assay	Purification fold (F_3)
Solvent extraction	1000	0.03	1
Column chromatography	97	0.27	9
Semi-preparative HPLC	31	1.3	43

Specific inhibition activity (SIA) was determined by the ratio of zone of clearance to the amount of compound loaded in the well.

Docking of lauric acid to PknB and PstP

The list of membrane proteins, common in both virulent (H37Rv) and avirulent (H37Ra) strains of *M. tuberculosis*, for which the

Table 3. The EI-Mass, ^{1}H-NMR and antimycobacterial activity by plate assay and MABA of the subfractions F_3, F_4 and F_5.

	EI-Mass spectrometry (*m/z*)			Antimycobacterial activity	
Subfractions	For the subfraction	NIST database	Peak integral values of the resonances observed in the ^{1}H NMR spectrum (0.75–2.5 ppm)	Zone of clearance* (mm) in agar well diffusion assay	MIC (µg/mL) by MABA
F_3	200.03	200.31	2.00, 2.04, 16.40, 2.90	28.0 ± 1.4	22.3 ± 0
F_4	228.04	228.37	2.00, 2.04, 20.22, 3.22	20.0 ± 1.4	66.7 ± 2.8
F_5	256.07	256.42	2.00, 2.39, 23.52, 3.10	12.0 ± 2.8	–

*The zone of clearance was measured with the 100 µg of the phytochemical.

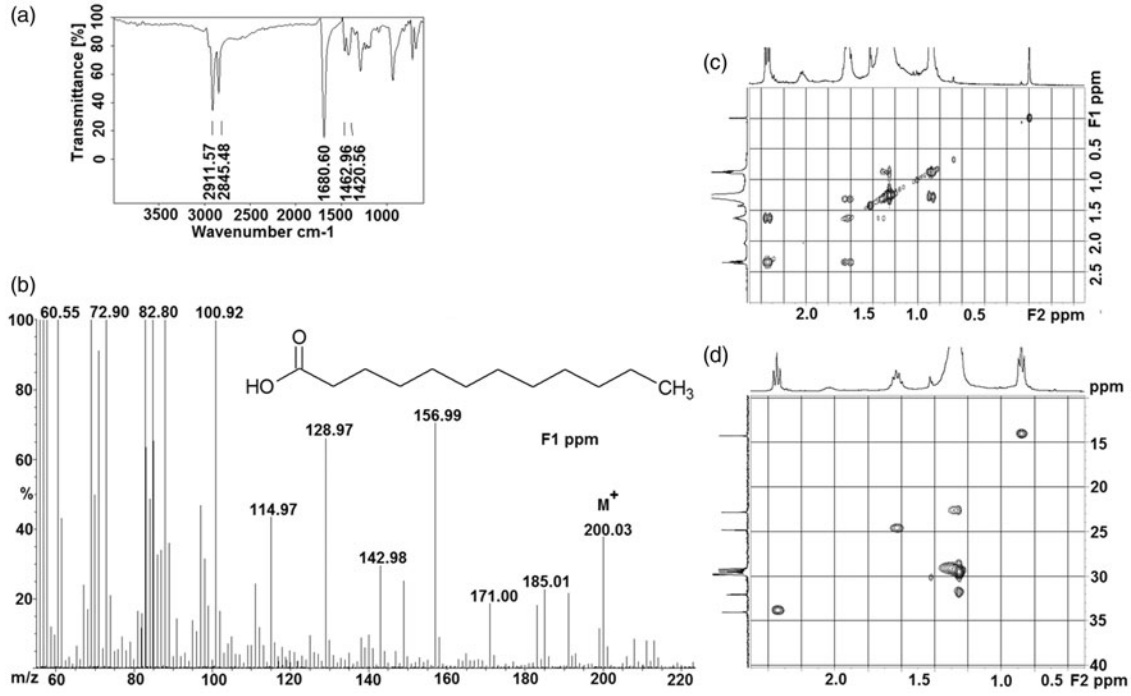

Figure 2. (a) IR spectrum, (b) EI-MS, (c) COSY (expanded spectrum), (d) HSQC (expanded spectrum) in $CDCl_3$ for the bioactive subfraction (F_3).

Table 4. The protein IDs, gene name and PDB codes for 12 membrane proteins are shown.

Protein IDs	Gene name	Protein description	PDB IDs
Rv1926c	*mpt63*	Immunogenic protein	1LMI
Rv2878c	*mpt53*	Soluble secreted antigen MPT53 precursor	1LU4
Rv0014c	*PknB*	*Transmembrane serine/threonine protein kinase B*	*1MRU, 3ORM, 3ORI, 3F61, 3F69, 1O6Y*
Rv0931c	*pknD*	Transmembrane serine/threonine protein kinase D	1RWI, 1RWL
Rv3804c	*fbpA*	Secreted antigen 85-A (Mycolyltransferase)	1SFR
Rv0129c	*fbpC*	Secreted antigen 85-C	1VA5, 1DQY, 1DQZ, 3HRH
Rv0983	*pepD*	Probable serine protease	1Y8T, 2Z9I
Rv0902c	*prrB*	Two component sensor histidine kinase	1YS3, 1YSR
Rv2945c	*lppX*	Probable conserved lipoprotein	2BYO
Rv0018c	*pstP*	*Possible PstP PPP*	*2CM1, 1TXO*
Rv2537c	*aroD*	3-Dehydroquinate dehydrastase	2DHQ, 1H05, 1H0S, 1H0R
Rv0985c	*mscL*	Possible large-conductance ion mechanosensitive	2OAR

The row having italic font contains the possible proteins responsible for signal transduction.

three-dimensional structures are known is given in Table 4 (Hiwa et al. 2011). The superimposed structure of the modelled full-length protein on the original truncated protein of PknB (1MRU) is given in Figure 3.

In order to derive unbiased information on the possible ligand binding site in PknB and PstP, blind docking procedure was adapted. One-hundred structures were generated and a root mean square (RMS) tolerance of 4 Å was set to form a cluster. In each cluster, structures were ranked by their binding energy. The best docked conformation was selected based on the lowest binding energy and with higher number of conformations in a given cluster (Rohit et al. 2009). It was observed that PknB displayed efficient binding (binding energy of −5.14 kcal/mol) with LA (Table 5).

Moreover, cluster analysis revealed that 56% of PknB–LA complex have the lowest binding energy compared to 13% for PstP–LA complexes. Additionally, identical binding regions were observed in both the clusters representing PknB–LA complex. These inferences indicate that LA could have greater preference for binding to PknB than PstP-LA.

Binding site residues

The frequency of occurrence of a given amino acid in the LA binding site of PknB is given in Table 6. It could be seen that the amino acid residues Val28, Lys43, Met148, Met158 and Asp159 are involved in all the 71 conformations. Moreover, the ligand binding site in PknB was predicted using 3DLigandSite server (http://www.sbg.bio.ic.ac.uk/3dligandsite/) (Wass et al. 2010). It was observed that the amino acids Leu20, Gly21, Phe22, Gly23, Gly24, Met25, Ser26, Val28, Ala41, Lys43, Met95, Glu96, Tyr97, Val98, Thr102, Ala145, Asn146, Met148, Met158 and Asp159 were presented in the predicted binding site. This site was identical to the binding region of KT5720 reported earlier (Carl et al. 2008).

Figure 4 depicts the binding mode of PknB with LA. Amino acid residues Lys43 and Asp159 in the activation loop of PknB were found to interact with the carboxylic group of LA.

Effect of chain length

In order to have a comprehensive understanding on the chain length dependency on the bi-molecular interaction, molecular docking was performed with other long-chain fatty acids. The results indicated that both lauric and MA interact with Lys43 and Asp159. However, palmitic acid was found to interact only with Asp159 (Supplementary Figures 9) possibly because of the strain conferred by the increased length of the alkyl chain and therefore could fail to fit into the binding cavity of PknB. Clustering

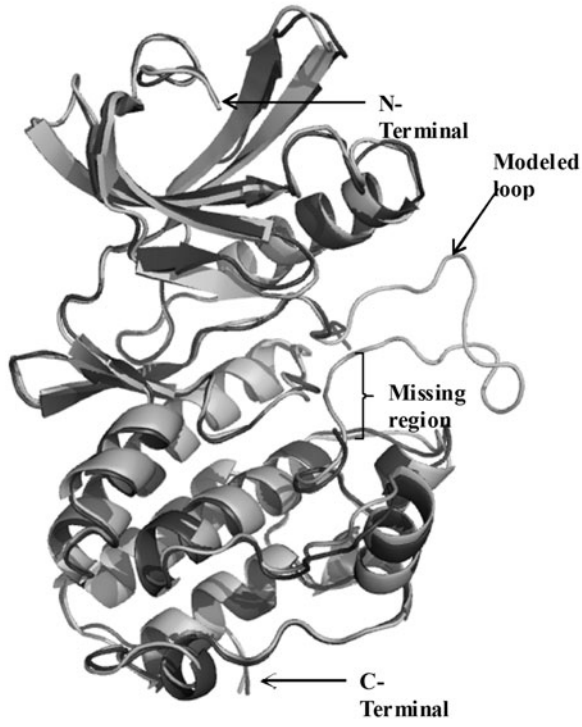

Figure 3. Superposition of the modeled cytosolic domain of PknB on the loop-deficient structure available at the PDB (PDB ID: 1MRU). The modeled loop region, present in between the N-terminal and C-terminal lobe is indicated.

analysis indicated that the number of conformations with lower binding energy decreases with increase in alkyl chain length, thus reflecting on its decreasing binding efficiency (Supplementary Table 2). However, the mean binding energy of lauric and MA was comparable.

Stability of the complex

The stability of PknB–LA complex was evaluated by performing molecular dynamic simulations. The RMSD of the simulated structures with respect to the initial structure is given in Figure 5. It could be seen that the RMSDs of both PknB and PknB-LA are stable after a simulation time period of 1500 ps, thus reflecting on their stability. However, the conformation of the amino acid residues in the ligand binding site seems to change upon binding to LA.

Discussion

LA, as approved by FDA, is a permitted food additive for human consumption as long as its concentration does not change the

Table 5. Results of lauric acid docking in PknB modeled structure (modeled 1MRU) and PstP (pdb code 2CM1) using Autodock 4.0 software.

	PknB-LA		PstP-LA				
Cluster rank	1	2	1	2	3	4	5
Lowest binding energy (kcal/mol)	−5.14	−3.79	−2.95	−2.89	−2.82	−2.79	−2.75
Mean binding energy (SD)	−4.32 (0.41)	−3.38 (0.36)	−2.72	−2.45	−2.36	−2.25	−2.15
Configurations in cluster	56	15	13	13	10	11	13

RMS-tolerance of 4 Å was considered for the clustering procedure, producing two and five distinct conformational clusters, out of 100 runs each. The first row indicates the number of the cluster, the lowest and mean binding energy values of each cluster are shown in the second and third rows, respectively. All energies are expressed in kilocalories/mole. The last row indicates the population of each cluster.
A threshold was set to >5 numbers of configurations in a cluster were chosen and displayed in order to avoid complexity.

Table 6. Binding site residues traced from the ligand with the distance of 4 Å using Swissprot deep viewer.

Binding site residues		L20	G21	G23	S26	V28	A41	K43	E62	V75	M95	E96	Y97	V98	M148	M158	D159
Frequency of occurrence (%)	Cluster rank 1	100	44	–	–	**100**	58	**100**	50	–	89	61	11	80	**100**	**100**	**100**
	Cluster rank 2	96	20	–	–	**100**	100	**100**	27	47	73	83	–	83	**100**	**100**	**100**

Three clusters show conserved residues of V28, K43, M148, M158 and D159 (highlighted in bold) of which only K43 and D159 are involved in electrostatic interaction to LA. All the values are rounded off by ±0.5%.

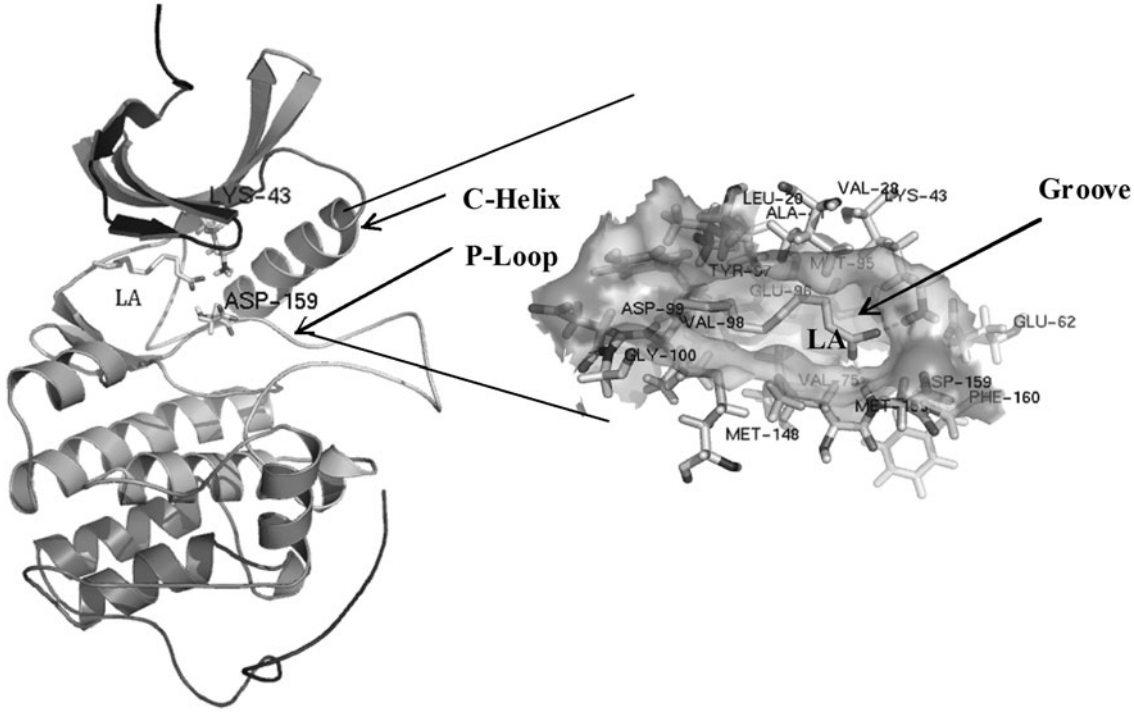

Figure 4. Proposed interaction of the mycobacterium PknB with LA. Intermolecular electrostatic interaction involving the amino acid residues, Lys43 and Asp159, is highlighted.

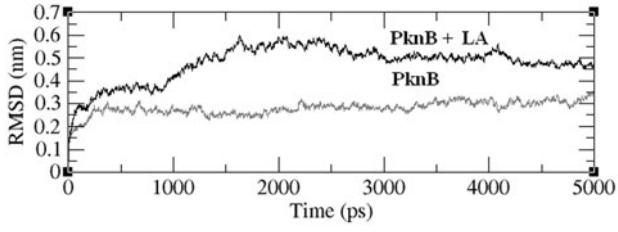

Figure 5. Variation in the RMSD values (*y*-axis) of all the backbone atoms as a function of simulation time (in ps). The data were acquired with a time interval of 5 ps.

physical, chemical and other technical effect of the food. In pharmaceutical applications, LA attachment enhances the bioavailability of certain drugs (Kravchenko et al. 2003). It also has the ability to control mastitis, an infection caused by *Staphylococcus aureus* (Kelsey et al. 2006). Antimycobacterial assay as well as molecular docking analysis emphasizes that LA is very effective in inhibiting the growth of *M. tuberculosis*. Studies on bioactivity of the molecules using agar well diffusion assay is of limited value (Collins & Franzblau 1997) and, in certain instances, may not reflect the real biological activity of the molecules. Diffusion of the molecules in the agar medium is the major rate limiting step and therefore cannot be used for any quantitative analysis. With this in view, in the present study, the antimycobacterial effect of the long chain fatty acids was analyzed both by agar well diffusion assays and by MABA. It should be noted that in both the assays, the inhibition activity of these fatty acids is indirectly proportional to the chain length, with LA being the most potent molecule to display this property. However, it should be mentioned that Kondo and Kanai (1977) and Saravanakumar et al. (2008) indicated greater antimycobacterial activity for

myristic acid. Direct correlation of the carbon chain length was also observed previously with regard to the cytotoxicity (with respect to leukemic cell lines) of these fatty acids (Lima et al., 2002). In addition to LA, MA extracted from other sources has been shown to possess antimycobacterial activity (Saravanakumar et al. 2008).

Among the long chain fatty acids used in the present study, the antimicrobial activity of MA is well documented (Miller et al. 1977; Skrivanova et al. 2006; Huang et al. 2011). It is present in the catalytic subunit of cyclic AMP-dependent protein kinase. MA can form N-myristylated protein by the catalytic enzyme N-myristyl transferase (Aitken et al. 1982; Carr et al. 1982). N-myristoylation is a co-translational modification involved in protein–protein interactions as well as in anchoring polypeptides to phospholipid bilayers by covalently attached to its N-terminus for proper protein localization or biological function; however, its role in targeting proteins to specific subcellular compartments has not been clearly defined (Peitzseh & MeLaughlin 1993; Michael et al. 1996). MA has also been indicated that myristoylated reductase localizes to mitochondria and endoplasmic reticulum by different mechanisms, and reveals a novel role for MA in protein targeting (Borgese et al. 1996). However, sufficient information on the exact mode of action of other long-chain fatty acids is not available. Also, the involvement of other fatty acids in the post-translational/co-translational modification of proteins is unknown. Supportively, a few of these fatty acids have been shown to interfere in the signal transduction process of the selected prokaryotic organisms and mammalian cells, thus affecting the growth and proliferation of the cell (Tommy et al. 1992; Tyagi & Deepak 2004; Yogesh et al. 2014).

In *M. tuberculosis*, the protein kinase family of proteins (PknA-PknG) have been shown to play crucial role in the bacterial survival or growth and therefore considered as one of the factor contributing to virulence. The membrane-bound members of Pkn family share greater homology in their sequence and therefore their domain organization. The cytosolic domain of this group of proteins possesses Ser/Thr kinase activity. Based on the information on the inhibition of signal transduction process and the importance of Pkn family in *M. tuberculosis,* we embarked on investigating the possible binding mode of these selected alkyl fatty acids to Pkn family of proteins in *M. tuberculosis*. Sequence alignment of PknB with the other members of this group indicates conservation of the two amino acids, Lys43 and Asp159, which are involved in electrostatic interaction with the fatty acid. Also, the enlarged binding site contains Leu20, Gly21, Val28, Ala41, Glu62, Val73, Val75, Glu96, Tyr97, Val98, Met148 and Met158, thus making hydrophobic contact with the alkyl chain. Though blind docking was used to dock the ligand, approximately 80% of the binding site residues correlate with predicted binding site residues (according to 3DLigandSite). Residues Lys140-Ile146 comprises the activation loop of PknB, which functions to coordinate with either Mg^{2+} or Mn^{2+} ion (Young et al., 2003). The molecular modelling also indicates that both the length of the alkyl chain and the carbonyl group plays vital role in the molecular recognition.

Conclusions

The present study, for the first time, authenticates the antimycobacterial property of long-chain fatty acids, especially LA and MA extracted from *A. sativum*. It is proposed that these molecules could possibly interfere with the signal transduction process of *M. tuberculosis* (H37Ra) by binding to PknB and its variants. However, more detailed analysis need to be carried out to have an in-depth understanding on the *in vivo* significance of this bimolecular interaction.

Acknowledgements

We acknowledge SIF, VIT University, Vellore (India) for extending the NMR, IR facility. We thank SAIF (IITM) for EI-MS. We also thank Mr. Vincent Sagayaraj from St Joseph College, Trichy, for their help in the semi-preparative HPLC. The authors thank the management of VIT University for providing the necessary infrastructure facility to carry out this work.

Disclosure statement

The authors report no declarations of interest.

References

Aitken A, Cohen P, Santikarn S, Williams DH, Calder AG, Smith A, Klee CB. 1982. Identification of the NH2-terminal blocking group of calcineurin B as myristic acid. FEBS Lett. 150:314–318.

Berendsen HJC, Van der Spoel D, Van Drunen R. 1995. GROMACS: a message-passing parallel molecular dynamics implementation. Comput Phys Commun. 91:43–56.

Borgese N, Aggujaro D, Carrera P, Pietrini G, Bassetti M. 1996. A role for N-myristoylation in protein targeting: NADH-cytochrome b5 reductase requires myristic acid for association with outer mitochondrial but not ER membranes. J Cell Biol. 135:1501–1513.

Bueno-Sánchez JG, Martínez-Morales JR, Stashenko EE, Ribón W. 2009. Antituberculosis activity of eleven aromatic and medicinal plants occurring in Colombia. Biomedica. 29:51–60.

Carl M, Anthony TI, Tom A. 2008. Auto-activation mechanism of the *Mycobacterium tuberculosis* PknB receptor Ser/Thr kinase. EMBO J. 27:3186–3197.

Carr SA, Biemann K, Shoji S, Parmelee DC, Titani K. 1982. n-Tetradecanoyl is the NH2-terminal blocking group of the catalytic subunit of cyclic AMP-dependent protein kinase from bovine cardiac muscle. Proc Natl Acad Sci USA. 79:6128–6131.

Chaudhar RD. 1996. Herbal drug industry. New Delhi: Eastern Publishers.

Collins LA, Franzblau SG. 1997. Microplate alamar blue assay versus BACTEC 460 system for high-throughput screening of compounds against *Mycobacterium tuberculosis* and *Mycobacterium avium*. Antimicrob Agents Chemother. 41:1004–1009.

Dario G, Roberto S. 2009. Improving accuracy and efficiency of blind protein-ligand docking by focusing on predicted binding sites. Proteins. 74:417–424.

Delaha EC, Garagusi VF. 1985. Inhibition of mycobacterial by garlic extract (*Allium sativum*). Antimicrob Agents Chemother. 27:485–486.

Dini C, Fabbri A, Geraci A. 2011. The potential role of garlic (*Allium sativum*) against the multi-drug resistant tuberculosis pandemic: a review. Ann Ist Super Sanita. 47:465–473.

Dye C, Scheele S, Dolin P, Pathania V, Raviglione MC. 1999. Consensus statement. Global burden of tuberculosis: estimated incidence, prevalence, and mortality by country. WHO Global Surveillance and Monitoring Project. JAMA. 282:677–686.

El-Sheakh AR, Ghoneim HA, Suddek GM, Ammar ESM. 2016. Attenuation of oxidative stress, inflammation, and endothelial dysfunction in hypercholesterolemic rabbits by allicin. Can J Physiol Pharmaco. 94:216–224.

Gebreyohannes G, Gebreyohannes M. 2013. Medicinal values of garlic: a review. Int J Med Sci. 5:401–408.

Global tuberculosis report. 2013. Report global tuberculosis control: surveillance, planning, financing. World Health Organization: Geneva, Switzerland; [cited 2015 April 20]. Available from http://apps.who.int/iris/bitstream/10665/91355/1/9789241564656_eng.pdf.

Global tuberculosis report. 2014. Drug-resistant TB surveillance & response, World Health Organization; [cited 2015 April 20]. Available from http://apps.who.int/iris/bitstream/10665/137094/1/9789241564809_eng.pdf.

Gupta R, Thakur B, Singh P, Singh HB, Sharma VD, Katoch VM, Chauhan SVS. 2011. Anti-tuberculosis activity of selected medicinal plants against multi-drug resistant *Mycobacterium tuberculosis* isolates. Ind J Med Res. 131:809–813.

Harborne JB. 1973. Phytochemical methods. London: Chapman and Hall Ltd, 49–188.
Hiwa M, Gustavo ADS, Sharad P, Tina S, Harald GW. 2011. Comparison of membrane proteins of *Mycobacterium tuberculosis* H37Rv and H37Ra strains. BMC Microbiol. 11:18.
Hu X, Shelver WH. 2003. Docking studies of matrix metalloproteinase inhibitors: zinc parameter optimization to improve the binding free energy prediction. J Mol Graph Model. 22:115–126.
Huang CB, Altimova Y, Myers TM, Ebersole JL. 2011. Short- and medium-chain fatty acids exhibit antimicrobial activity for oral microorganisms. Arch Oral Biol. 56:650–654.
Jain RC. 1998. Anti tubercular activity of garlic oil. Indian J Pathol Microbiol. 41:131.
Kelsey JA, Bayles KW, Shafii B, McGuire MA. 2006. Fatty acids and monoacylglycerols inhibit growth of *Staphylococcus aureus*. Lipids. 41:951–961.
Kondo E, Kanai K. 1977. The relationship between the chemical structure of fatty acids and their mycobactericidal activity. Jpn J Med Sci Biol.30:171–178.
Kouznetsov VV, Sánchez JGB. 2010. Antimycobacterial susceptibility testing methods for natural products research. Braz J Microbiol. 41:270–277.
Kravchenko IA, Golovenko NY, Larionov VB, Aleksandrova AI, Ovcharenko NV. 2003. Effect of lauric acid on transdermal penetration of phenazepam *in vivo*. Bull Exp Biol Med. 136:579–581.
Lanos GG, Araujo LM, Jiménez IA, Moujir LM, Bazzocchi IL. 2012. Withaferin A-related steroids from *Withania aristata* exhibit potent antiproliferative activity by inducing apoptosis in human tumor cells. Eur J Med Chem. 54:499–511.
Lima TM, Kanunfre CC, Pompeia C, Verlengia R, Curi R. 2002. Ranking the toxicity of fatty acids on Jurkat and Raji cells by flow cytometric analysis. Toxicol In Vitro. 16:741–747.
Michael TK, Howard B, Frank R. 1996. Contributions of Myristoylation to calcineurin structure/function. J Biol Chem. 271:26517–26521.
Middlebrook G, Cohn ML. 1958. Bacteriology of tuberculosis: laboratory methods. Am J Public Health Nations Health. 48:844–853.
Mikaili P, Maadirad S, Moloudizargari M, Aghajanshakeri S, Sarahroodi S. 2013. Therapeutic uses and pharmacological properties of garlic, shallot, and their biologically active compounds. Iran J Basic Med Sci. 16:1031–1048.
Miller RD, Brown K, Morse SA. 1977. Inhibitory action of fatty acids on the growth of *Neisseria gonorrhoeae*. Infect Immun.17:303–312.
Molina-Salinas GM, Pérez-López A, Becerril-Montes P, Salazar-Aranda R, Said-Fernández S, Waksman de Torres N. 2007. Evaluation of the flora of northern Mexico for *in vitro* antimicrobial and antituberculosis activity. J Ethnopharmacol. 109:435–441.
Newton SM, Lau C, Wright CW. 2000. A review of antimycobacterial natural products. Phytother Res. 14:303–322.
Parish T, Stroker NG. 1998. Mycobacteria protocols: methods in molecular biology. Totowa (NJ): Humana Press.
Patra JK, Gouda S, Sahoo SK, Thatoi HN. 2012. Chromatography separation, 1H NMR analysis and bioautography screening of methanol extract of *Excoecaria agallocha* L. from Bhitarkanika, Orissa, India. Asian Pac J Trop Biomed. 2:S50–S56.
Peitzseh RM, MeLaughlin S. 1993. Binding of acylated peptides and fatty acids to phospholipid vesicles: pertinence to myristoylated proteins. Biochem. 32:10436–10443.
Prescott ML, Harley J, Donald P, Klein A. 1999. Microbiology. 2nd ed. TX: Brown Publisher. p. 325.
Rajiniraja M, Jayaraman G. 2014. Bioautography guided screening of selected Indian medicinal plants reveals potent antimycobacterial activity of *Allium sativum* extracts – implication of non sulfur compounds in inhibition. Int J Pharm Pharm Sci. 6:671–676.
Rohit T, Kiran M, Ryan P, Chenglong L, Werner T. 2009. Carborane clusters in computational drug design: a comparative docking evaluation using Autodock, Flexx, Glide and Surflex. J Chem Inf Model. 49:1581–1589.
Saravanakumar DEM, Folb PI, Campbell BW, Smith P. 2008. Antimycobacterial activity of the red alga *Polysiphonia virgata*. Pharm Biol. 46:254–260.
Schauenberg P, Paris F. 1990. Guide to medicinal plants. First paperback edition, Paris: Lutterworth Press.
Schuler LD, Daura X, Van Gunsteren WF. 2001. An improved GROMOS96 force field for aliphatic hydrocarbons in the condensed phase. J Comput Chem. 22:1205–1218.
Schuttelkopf AW, Van Aalten DMF. 2004. PRODRG: a tool for high-throughput crystallography of protein-ligand complexes. Acta Crystallogr D. 60:1355–1363.
Shigemi Z, Furukawa Y, Hosokawa K, Minami S, Matsuhiro J, Nakata S, Watanabe T, Kagawa H, Nakagawa K, Takeda H, et al. 2016. Diallyl trisulfide induces apoptosis by suppressing NF-κB signaling through destabilization of TRAF6 in primary effusion lymphoma. Int J Oncol. 48:293–304.
Skrivanova E, Marounek M, Benda V, Brezin P. 2006. Susceptibility of *Escherichia coli*, Salmonella sp. and *Clostridium perfringens* to organic acids and monolaurin. Vet Med – Czech. 51:81–88.
Tommy N, Tomas M, Tiina P, Leif CA. 1992. Modulation of calcium fluxes in Jurkat T cells by myristic acid inhibition is independent of membrane potential and intracellular pH. Biochem J. 283:113–118.
Tyagi JS, Deepak S. 2004. Signal transduction systems of mycobacteria with special reference to *M. tuberculosis*. Curr Sci. 86:93–102.
Wass MN, Kelley LA, Sternberg MJ. 2010. 3DLigandSite: predicting ligand-binding sites using similar structures. Nucleic Acids Res. 38:469–473.
Yogesh C, Sandeep U, Shazia K, Sathya Narayanan N, Francesca F, Vinay Kumar N. 2014. Protein Kinase B (PknB) of *Mycobacterium tuberculosis* is essential for growth of the pathogen *in vitro* as well as for survival within the host. J Biol Chem. 289:13858–13875.
Young TA, Delagoutee B, Endrizzi JA, Falcik AM, Alber T. 2003. Structure of *Mycobacterium tuberculosis* PknB supports a universal activation mechanism for Ser/Thr protein kinases. Nat Struct Biol.10:168–174.
Zhang B, Li F, Zhao W, Li J, Li Q, Wang W. 2015. Protective effects of allicin against ischemic stroke in a rat model of middle cerebral artery occlusion. Mol Med Rep. 12:3734–3738.